Physica B: Condensed Matter 568 (2019) 51–59

Contents lists available at ScienceDirect

Physica B: Condensed Matter

journal homepage: www.elsevier.com/locate/physb

Enhanced electrochemical studies of ZnO/CNT nanocomposite for supercapacitor devices

R. Ranjithkumar[a], S. Ezhil Arasi[a], S. Sudhahar[b], N. Nallamuthu[a,*], P. Devendran[a], P. Lakshmanan[c], M. Krishna Kumar[a,**]

[a] Department of Physics, International Research Centre, Kalasalingam Academy of Research and Education, Krishnankoil-626126, Tamil Nadu, India
[b] Department of Physics, Alagappa University, Karaikudi - 630003, Tamil Nadu, India
[c] Department of Chemistry, Kalasalingam Academy of Research and Education, Krishnankoil-626126, Tamil Nadu, India

ARTICLE INFO

Keywords:
ZnO/CNT
Conventional chemical reflux
Electrochemical studies
Energy storage devices
Supercapacitor

ABSTRACT

ZnO nanorods embedded on functionalized CNT have been synthesised by the chemical refluxing method. The characterization results revealed the tube-like structure of carbon nanotubes, that expose the ZnO nanorods grafted upright and parallel on the floor across the CNT surface. The powder X-ray diffraction patterns show that crystalline ZnO nanorods are highly loaded on the surface of CNT and formed as a nano-composite. Raman spectroscopy results showed that the intensity of D and G bands decreased due to the loading of ZnO nanorods. Cyclic voltammetry curves reveal the double layer capacitor (EDLC) behaviour of ZnO/CNT. The synthesised hybrid ZnO/CNT exhibits a high specific capacitance (SPc) of 189 Fg^{-1}. The quick charge-discharge performance was found about 95 Fg^{-1} and the cyclic stability of 96% was observed for 1000 cycles. ZnO/CNT nano-composites also exhibit a high power density of 2250 W kg^{-1}.

1. Introduction

The growing demand for instant power supply sources like supercapacitors, ultracapacitors, etc., accelerate research attention on well-defined pathways of ions/electronic transports [1,2]. Designing novel hybrid electrode matrix materials by hosting large surface area nano-systems with materials of high specific capacitance offer high power density cater to the needs in hybrid vehicles and versatile electronic applications [3]. Moreover, high alert of environmental pollution hungers clean, sustainable and efficient energy storage and conversion technologies for next-generation applications, such as electric vehicles (EV), Hybrid vehicles,etc., [4,5]. The materials showing very long cyclic life, high power density are the abrupt need for supercapacitors and ability of a large amount of electrical energy stored hybrid materials are the contemporary interest of among world researchers for future technological advancements [6,7].

The energy storage is purely the ability of materials own quality, which is driven by accumulating electrostatic charge at the surface of electrodes (Non-Faradic process) and reversible oxidation and reduction process (Faradaic process) on the surface of electrodes.

It occurs between the electrodes in the optimized electrolyte interfaces [8,9]. Wherever a quick charge is needed to fill a short term power need, the supercapacitors are ideal, whereas batteries are chosen to provide long-term energy need and it will be used for different load levelling applications [10–12]. They are most effective to bridging power gaps lasting from a few seconds to a few minutes and can be recharged quickly. Generally, supercapacitors have high self-discharge property which is higher than most batteries and low cell voltage [13].

The active surface area of porous carbon can be altered by effective acid treatments and provide space cater to the high specific capacitance (SPc). The control of porous nature, surface area and grafting the metal oxides onto the highly conductive carbon materials such as graphene, carbon nanotubes, and activated carbon is a challenging work to evolve an efficient electrode material [14–16]. The doping process of non-carbon atoms will induce defects in the tubular lattice of carbon nanotubes (CNT) and chemical reactivity in the carbon nanotube surface increases. The oxidation of CNT is widely performed with oxidant agents such as HNO_3, H_2SO_4, $KMnO_4$ and H_2O_2 in various synthesis methods. It has been observed that, under oxidation process, a variety of functional groups such as (-COOH, –C═O, –OH) are formed on the surface of CNT and that promotes CNT chemical reactivity to link with other ligands. The oxides functionalization process enables dispersibility of CNT in aqueous and organic solvents and thus it can be directly used of composite synthesis. The outstanding mechanical

* Corresponding author.
** Corresponding author.
E-mail addresses: n.nallamuthu@klu.ac.in, nnallamuthu@gmail.com (N. Nallamuthu), krishnakumarinfo@gmail.com (M.K. Kumar).

https://doi.org/10.1016/j.physb.2019.05.025
Received 11 April 2019; Received in revised form 13 May 2019; Accepted 14 May 2019
Available online 16 May 2019

property and high surface to volume ratio of carbon nanotubes (CNT) make it ensure the utmost exploration to fabricate hybrid composite electrode materials [17,18]. The harsh treatment of CNT can be destructive to the network, damaging side walls and may cut the structure. But the facile surface modification of CNT by reflux method does provide the possibility to attach external moieties through covalent bond without changing its fundamental structure and its bulk properties [19–22].

The pseudocapacitive transition metal oxides of MnO_2 [23,24], NiO [25], Co_3O_4 [26,27], $Ni(OH)_2$ [28,29], $Co(OH)_2$ [30], RuO_2 [31], and $NiCo_2O_4$ [32] have an extensive attention and much efforts have been taken on them, due to their higher specific capacitance in-order to increase double layer capacitance of carbon-based materials. Their hybrid forms of metal oxides/carbon materials are also reported to be outstanding for electrochemical storage devices [33]. Even though many efforts have been taken on metal oxides, high specific capacitance coupled with good cyclic performance on conducting carbon materials is still challenging.

The oxidation-reduction process of ZnO offers faster movements of electrons and it gives the advanced design of CNT based electrochemical applications. The association of carbon nanotubes (CNT) with ZnO nanorods is proposed in this research work due to the special characteristics of CNT that can be utilized to increase the electrochemical activity.

Aravinda et al. fabricated highly loaded ZnO in film form (thickness 186 nm) on CNT material by DC magnetron sputtering technique to obtain a SPc value of 59 F/g [33]. Ramli et al. reported hydrothermally derived ZnO/CNT/GNF (ZnO 40 wt%) which exhibited a specific capacitance value of 306 F/g [34]. In addition, Zhang et al. was applied spray pyrolysis technique to prepare CNT-ZnO. In this sample, Zinc Oxide was randomly dispersed on the surface of CNT and exhibited a SPc value of 126.3 F/g [35]. Venugopal et al. simply applied hydrothermally derived ZnO on CNT by mixing. In their study, ZnO/CNT (1:2 wt ratio) showed a SPc value of 23.2 F/g. In this case, zinc oxide nanoparticles are present in very broad size distribution (20–200 nm) [36]. Lee et al. employed hydrothermal method, in which ZnO particles grown in the presence of CNT in solution phase. But, the FE-SEM results revealed that, the presence of very large sized zinc oxide particles (> 500 nm) and that sample exhibited a SPc value of 40.1 F/g [37]. The aforementioned methods like pyrolysis, simple mixing, and hydrothermal methods have resulted into low-values of SPc [38]. It was declared that, the broad size distribution of ZnO particles and the presence to the isolated ZnO phase could be the reasons for the observed lower SPc. The comparison of results is given in Table 1. The oxidization treatment of CNT with HNO_3, $KMnO_4/H_2SO_4$, $K_2Cr_2O_7/H_2SO_4$ will open the CNT faces and cut into short tubes [39]. In the meantime, defects were introduced around the CNT surface, which will increase the reaction ability of CNT. Loading of ZnO nanorods on CNT can be an interesting candidate for electrochemical applications.

In the present study, highly loaded ZnO/CNT nanocomposites were prepared by one-pot synthesis. This involves a typical chemical refluxing method and functionalized CNT. The chemical refluxing method resulted in the formation of ZnO nano-rods (aspect ratio ~ 3) grown perpendicular to the surfaces of CNT. The present research work material synthesis approach is quite different from previously reported results (Table 1) and hence, title composite ZnO/CNT is novel for supercapacitor applications. The planting of such ZnO nanorods in large number on the CNT surface results in dramatic improvement of specific capacitance. The improvement in the specific capacitance has been discussed in the light of characterization.

2. Materials and methods

2.1. Functionalization of CNT

Carbon nanotubes (CNT) and zinc nitrate [Zn $(NO_3).6H_2O$] were purchased from Sigma-Aldrich and used as received. The facial functionalization of CNT was performed at 120 °C by applying chemical refluxing method. In a typical process, 150 mg of CNT was added into a mixture of de-ionized water and nitric acid (HNO_3) with a ratio of 1:1.5.

The solution was continuously stirred 1 h for mixing well followed by sonication (1 h) for achieving homogenously dispersed CNT solution. Further, it was stirred 8 h at 120 °C to effect facial reaction on CNT by attaching the hydroxyl (OH) groups through the splitting of the hydronium (H_3O^+) ion. The long stirring leads to strong binding of hydroxyl groups with CNT carbon atoms by breaking the C=C in a ring. The obtained functionalized CNT (FCNT) precipitate was washed in de-ionized water and ethanol several times to achieve pure FCNT. Further, it was dried at 80 °C and used for further reactions.

2.2. Synthesis of ZnO/CNT

In a typical synthesis, 100 mg of functionalized CNT (FCNT) was dispersed in 80 ml de-ionized water in the round bottom flask (RB) by using sonication to make a homogenous solution. The 0.01 M of Zn $(NO_3).6H_2O$ solution was added into the FCNT solution and stirred 3 h at 120 °C. The calculated amount of NaOH (0.3 g) was dissolved separately in 20 ml de-ionized water and it was added drop-wise into FCNT solution. The constant temperature will be useful to maintain uniform-sized ZnO nanorods that will be embedded on the surface (might be parallel and vertical directions and possible to enter into the pores of CNT, that maybe depends on the duration of reflux and temperature). At this state, 0.01 M hexamine was added into the solution as a binding agent to avoid the removal of embedded ZnO in CNT. This chemical reflux process was continued about 3 h to ensure the implant of ZnO nanorods on the surface and inner of CNT cylinder. Precipitation of ZnO/CNT was collected and washed in de-ionized water and ethanol for few times to enrich the quality and same dried at 80 °C in vacuum for 10 h. ZnO/CNT was kept for spectral, structural and other characterizations to evaluate its physical identity and the rest is kept safe in desiccators for further use of electrode preparation. The synthesis representation in the functionalization of CNT and ZnO/CNT is shown in Fig. 1.

Table 1
Comparison of previous literature of ZnO/CNT composites

Material	Electrolyte	Scan rate (or) current density	Specific capacitance (Spc)	Method	Reference
CNT-ZnO	PVA/PMA	No data	126.3 Fg^{-1}	spray pyrolysis	35
ZnO/CNT nanocomposite	0.5 M KCl	100 mVs^{-1}	25.66 Fg^{-1}	simple mixing method	36
ZnO/MWNT composites	1 M tetraethylammonium tetrafluoroborate	5 mVs^{-1}	40 Fg^{-1}	hydrothermal method	37
CNT/GT/ZnO composites	1 M KCl	25 mVs^{-1}	6.99 Fg^{-1}	Sol-gel method	38
ZnO/FWNTs	Tetra butyl ammonium perchlorate in Dimethylforamide	5 mVs^{-1}	59 Fg^{-1}	DC magnetron sputtering	33
ZnO/CNT	1 M Na_2SO_4	1 mVs^{-1}	189 Fg^{-1}	Chemical reflux method	**This work**

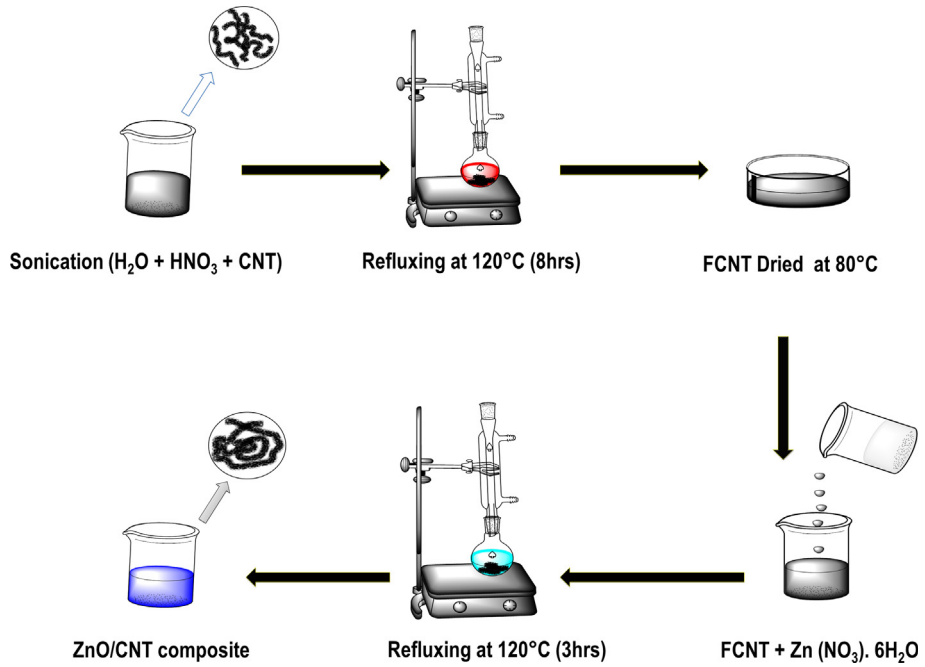

Fig. 1. Synthesis scheme of FCNT and ZnO/CNT.

2.3. Characterization methods

Powder X-ray diffraction pattern of CNT was examined by using Bruker instrument of model D8 advance ECO XRD systems with SSD160 1D Detector which has Cu-K_α radiation of wavelength 1.5406 Å. A scanning electron microscope ZEISS EVO 18 which was equipped with BRUKER X-Flash 6130 energy dispersive X-ray spectrometer was used to study the surface morphology of prepared sample and to record spectrum to confirm the composition of ZnO and CNT. An instrument Shimadzu IR Trace-100 spectrometer was used to record the infrared spectrum of prepared pure and Zinc embedded CNT samples by KBr pellet method. The electrochemical response of the pure CNT and Zinc embedded carbon nanotubes (CNT) electrodes were analysed in Na_2SO_4 electrolyte by using three electrodes system electrochemical work-station CHI6008E. The electrode of ZnO/CNT was prepared using 0.01 mm thick and 1 cm^2 Nickel foil for electrochemical performance analysis. Initially, the surface of Ni foil was rubbed with emery sheet and allowed for sonication, then cleaned with acetone. Activated carbon, ZnO/CNT, polyvinylidene fluoride (PVDF) binder was mixed with the weight ratio of 80:10:10 and ground well for mixing homo-geneous mixture. In addition, a drop of N-methyl-2- pyrrolidone (NMP) was added to the mixture to make it as slurry and then it was applied as a thin film on nickel foil. It was dried at 80 °C further; it was used to analyse the electrochemical characteristics of ZnO/CNT in 1 mol Na_2SO_4 as an electrolyte by three electrode system of electrochemical analyser CHI6008E model.

3. Results and discussion

3.1. ZnO/CNT structural studies

The powder X-ray diffraction pattern of ZnO embedded carbon nanotubes is depicted in Fig. 2. The observed crystalline peaks of ZnO has very closely matched with standard data (JCPDS card No: 79-2205) of ZnO. It shows that CNT has a shoulder peak at about 2θ of 25° and it is completely reduced its hump due to ZnO nanorods embedded on the entire surface of CNT. Fig. 2(a) shows a typical powder X-ray diffraction (PXRD) pattern oxidized CNT at 120 °C for 8 h. Fig. 2(b) shows the PXRD crystalline patterns of ZnO nanorods. Carbon nanotubes consist

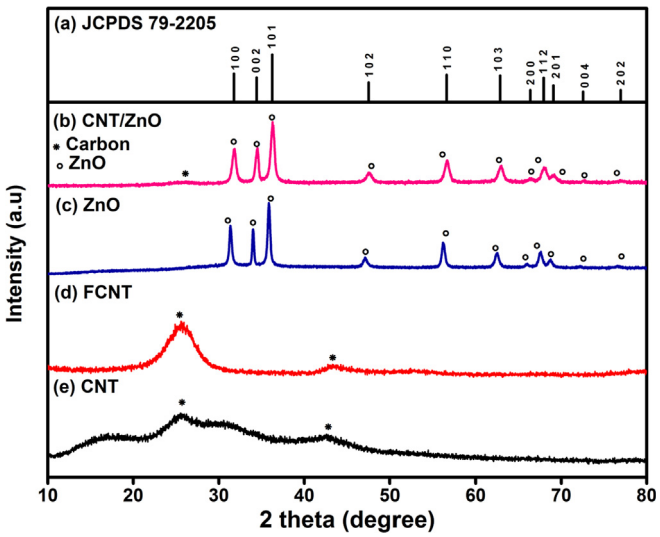

Fig. 2. Powder XRD patterns of CNT, FCNT, ZnO and ZnO/CNT.

of elongated tubular molecules, which only have the hexagonal rings. The strong diffraction peak at the angle (2θ) of 25.54° can be indexed as the C (002) reflection of the hexagonal graphite structure [40,41]. In actual, C–C bond length in graphite is 0.142 nm, and C=C double bond has a length of 0.134 nm. Another characteristic diffraction peak of Zinc Oxide was found at 2θ of about 43.2° [42]. Fig. 2 (b) shows a PXRD pattern of ZnO nanorod and its SAED pattern. The diffraction pattern can be indexed and excellent crystallinity of ZnO is confirmed. The diffraction peaks of synthesised ZnO nanorods have good agreement with JCPDS card no: 79-2205.

The quantum effect of nanotube-nanotube interactions, covalent carbon-carbon bonds behaviour was analysed by the vibrational modes of FT-IR spectra (Fig. 3) and laser Raman spectroscopy (Fig. 4). Fig. 2 shows that the FT-IR spectra of ZnO nanorods and ZnO/CNT separately in the range of 400–4000 cm^{-1}. The broad peak at 3386 cm^{-1} and a peak at 1637 cm^{-1} were assigned to O–H functional vibrations present on the ZnO rods surface.

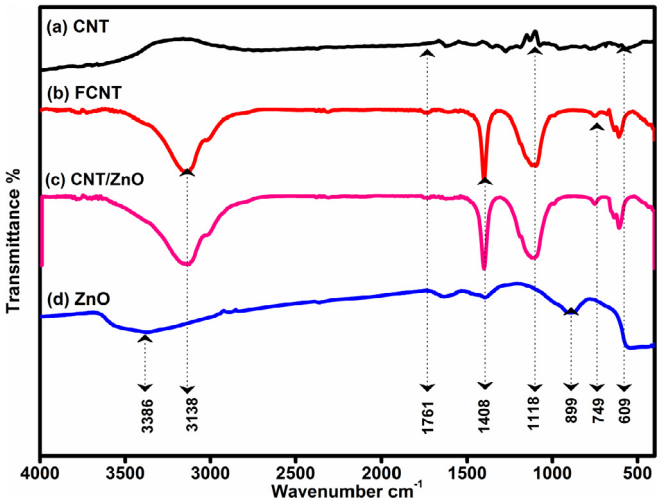

Fig. 3. FT-IR spectra of (a) pure CNT (b) FCNT (c) ZnO/CNT and (d) ZnO.

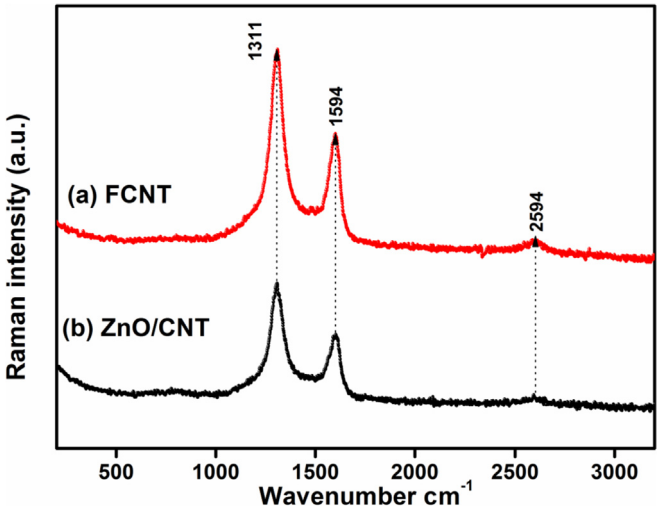

Fig. 4. FT-Raman spectra of (a) FCNT and (b) ZnO/CNT.

The vibration at 1637 cm^{-1} in ZnO nanorods is diminished as a weak signal when embedded with CNT. The stretching vibration found at 899 cm^{-1}confirms that Zn–O nanorods bond [43]. Fig. 3 (ZnO with CNT) shows that high intensity stretching vibration peak of the hydroxyl group (-OH) at 3138 cm^{-1}. The oxidized state of CNT was revealed by asymmetric C=O stretching vibration at 1761 cm^{-1}. The characteristic peak of ZnO metal oxide appears at 609 cm^{-1} [44]. The peak at 1118 cm^{-1} is attributed due to C–O bond stretching of oxidized CNT. The symmetric C–O–H stretching mode exhibits a peak at 1408 cm^{-1} [45].

The vibrational aspects of all sp^2 carbons, the diameter of nanotubes and the presence of disorder in sp^2 hybridized carbon systems were revealed by the Raman spectra. The vibrations of carbon nanotubes might be modified by the hosted molecule (OH) during HNO_3 functionalization. In Fig. 4, disorder-induced mode (G band) at 1594 cm^{-1} occurs due to in-plane tangential vibrations of C–C bond. A band at 1311 cm^{-1} (D band) was present due to the existing disorder in graphitic carbon systems [46]. The FWHM of D band of FCNT was found to be about 89 cm^{-1}, ZnO-CNT shows the FWHM about Raman shift of 88 cm^{-1}.

The HNO_3 structure contains oxygen atoms and it can be easily binding to the defects of CNT bond and which leads to greater modifications in the defect band and it was observed in Raman intensity (Fig. 4). The signal G′ band is present at 2594 cm^{-1} due to two-phonon second-order scattering process and it is indicating the existence of long-range order in a CNT [47].

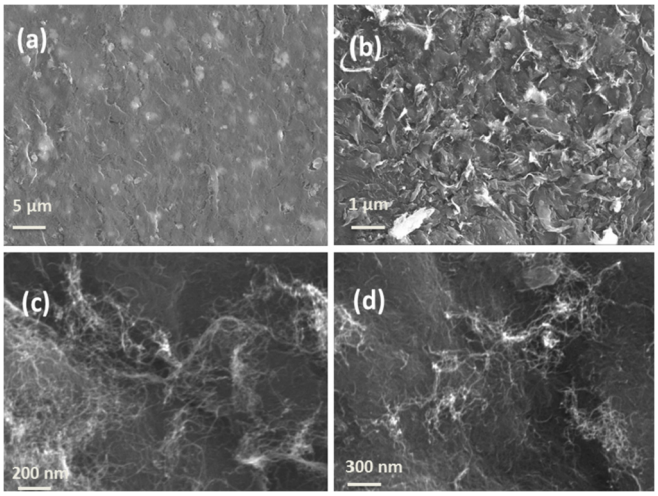

Fig. 5. SEM images of FCNT with different magnifications.

3.2. Surface studies and elemental mapping

The surface images of the oxidized CNT was recorded by scanning electron microscope (SEM) and it is shown in Fig. 5(a–d) with different magnifications [(a) at 5 µm, (b) at 1 µm, (c) at 200 nm and (d) at 300 nm]. Fig. 6(a–d) shows scanning electron micrographs of a ZnO nanorods embedded on FCNT in different magnifications [(a) at 5 µm, (b) at 500 nm, (c) at 200 nm and (d) at 200 nm]. It clearly illustrates that the ZnO nanorods stand implanted on the surface of the oxidized CNT. ZnO nanorods sizes can be controlled by maintaining reflux temperature and spread over on the surface of CNT and it was confirmed by the SEM images (Fig. 6). It might be expected that enhanced cyclic voltammetry (CV) performance can arise from ZnO/CNT. The chemical stoichiometry of ZnO/CNT nanorods was investigated by EDX with mapping, which shows that oxygen content is enriched and it is about 28 wt percentage (Fig. 7(a-e)) [48,49]. Fig. 7(a, b) shows that EDS spectrum and elemental mapping of ZnO/CNT nanocomposites and Fig. 7(c–e) shown the individual elemental mapping of Carbon, Oxygen and Zinc respectively.

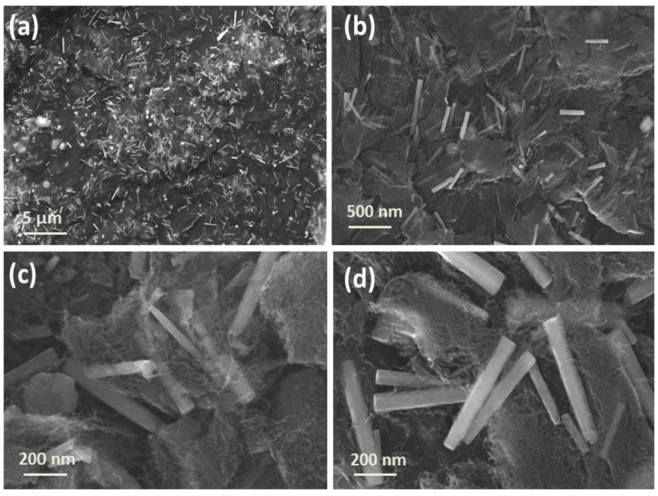

Fig. 6. SEM images of ZnO/CNT in different magnifications.

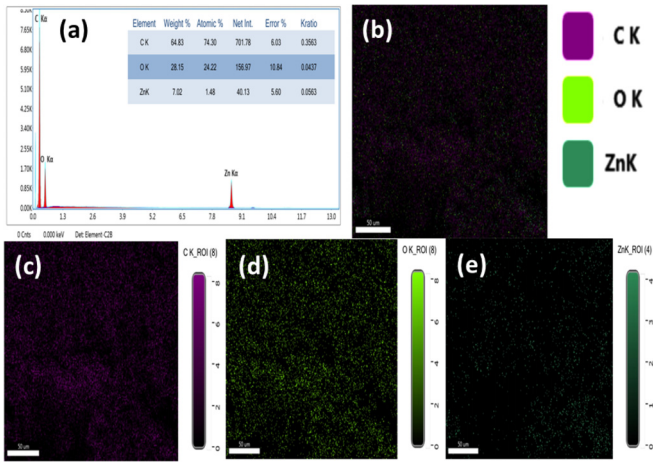

Fig. 7. EDAX analysis and mapping of ZnO/CNT.

3.3. Cyclic voltammetry results

The electrochemical activity of ZnO/CNT modified electrode was inspected by using the potentiostatic system of cyclic voltammetry [50]. The electrochemical behaviour of the Zn^{2+} redox reactions at the surface of CNT was studied in 1 M Na_2SO_4 electrolyte with different scan rates (1–100 mV s^{-1}) as shown in Fig. 8. The potential window was obtained in the range of −0.9 V to 0 V versus the current density for different (1–100 mV) scan rates. The rate capability of the electrode is remarkable and it shows that they maintain pseudocapacitive behaviour by exhibiting rectangular CV shape in lower voltages. The rectangular area of the CV curve varied from smaller applied voltages to higher voltages. The volumetric currents and area of the CV curve of the ZnO/CNT electrodes increase with scan rates due to an increase of pseudocapacitive/EDLC of ZnO, which results in increasing volumetric capacitance. The crystalline ZnO molecules in Na_2SO_4 electrolyte have redox process from the intercalation/dis-intercalation process of the cations, but it is interesting to observe that, ZnO/CNT does not show that no such redox peaks. The cyclic voltammetric (CV) curve in rectangular shape indicates EDLC behaviour. The total specific capacitance of ZnO/CNT arises from combined activity of pseudo behaviour of ZnO and EDLC behaviour of CNT, which results in no any distinct peaks of ZnO and CNT. This absence of redox peak is attributed due to charging and discharging at the pseudo-constant rate in the entire voltammetry cycle [51,52]. The rate-dependent cyclic voltammetry of ZnO/CNT electrode was depicted in Fig. 8. Consider the Fig. 8 (d). It clearly reveals that the current density of ZnO/CNT is higher than that of individual ZnO and CNT. These results show the beneficial effects of making a nano-composite of ZnO with CNT. The specific capacitance of value of $\boldsymbol{C_{sp} = \frac{\int \mathrm{I}\, dv}{vm\ \Delta \mathrm{V}}}$ the working electrodes has been calculated from the CV curves by using the following formulas (1) and (2),

$$C_{sp} = \frac{\int \mathrm{I}\, dv}{vm\ \Delta \mathrm{V}} \tag{1}$$

where $\int \mathrm{I}\, dv$ is the integral area under the cyclic voltametry curve, v is the scan rate (mVs^{-1}), m is the mass of electroactive materials, and ΔV is the potential window (V).

$$\boldsymbol{C_{sp} = \frac{I\ X\ \Delta T}{mX\ \Delta V}} \tag{2}$$

where 'm' is the mass of electroactive material, ΔV is the potential window (V), ΔT is the discharge time and I is the constant discharge current.

The specific capacitance values for scan rates 1–100 mV are calculated and it is depicted as a graph as shown in Fig. 9. The respective values for the scan rates are given in Table 2. At lower scanning rate 1 mVs^{-1}, active electrode surface area is more for involving in electrochemical reaction. But, when increasing scanning rate (5,10 mVs^{-1}), active surface area involving in electrochemical reaction will decrease and due to that, the specific capacitance decreases. When, compare the Fig. 8-d with Fig. 9, pure ZnO material exhibits the lowest range of current density (Fig. 8-d), which is in line with the lowest specific capacitance (Fig. 9). But pure CNT shows better results than that of ZnO. Interestingly, the ZnO/CNT composite material exhibits the highest specific capacitance (Fig. 9), which corroborates well with the observed current density (Fig. 8-d). It is observed that, uniformly grown ZnO nanorods embedded CNT (ZnO/CNT) revealed higher specific

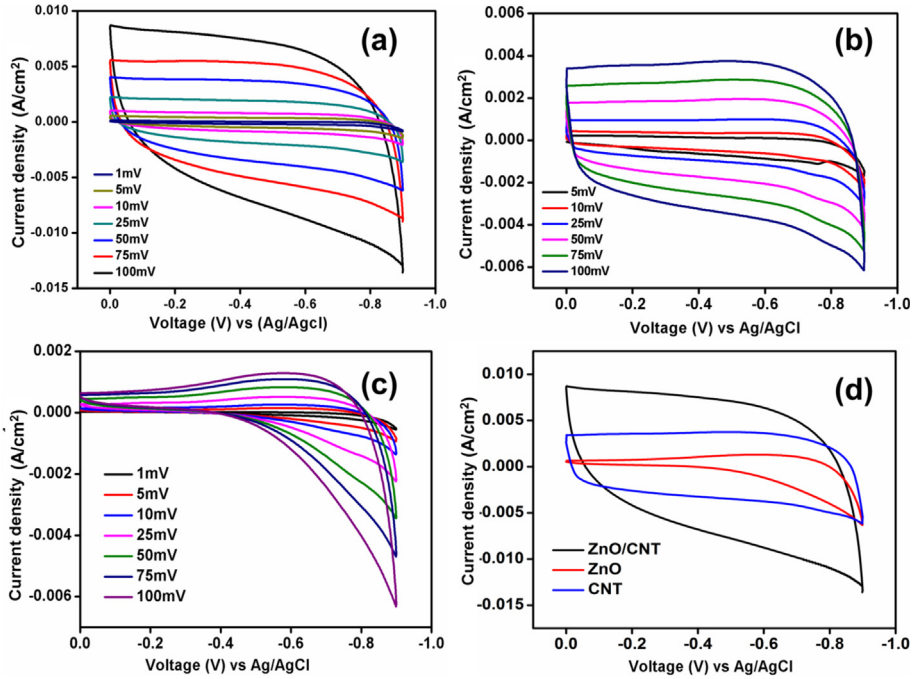

Fig. 8. Cyclic voltammetry curves of (a) ZnO/CNT in different scan mVs^{-1} (b) CNT in different scan mVs^{-1} (c) ZnO in different scan mVs^{-1} and (d) ZnO/CNT, ZnO and CNT in 100mVs^{-1}

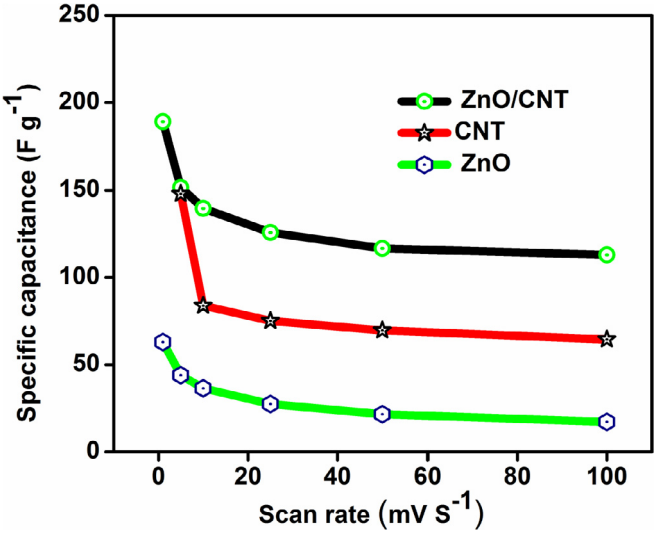

Fig. 9. Plot of specific capacitance vs. scan rate of ZnO/CNT nanocomposite.

Table 2
Specific capacitance (Fg^{-1}) values of ZnO/CNT at different scan rates.

Scan rate (mV S^{-1})	Specific capacitance (F g^{-1})
1	189
5	151
10	139
25	125
50	116
100	112

capacitance value of 189 F/g at 1 mVs^{-1}.

Also, In order to understand the cyclic stability of ZnO/CNT nanocomposites, the Galvanostatic charge-discharge (GCD) test was carried out. Fig. 10 shows GCD curves of ZnO/CNT at a constant current density about 10 mA/g, which indicates that optimal electrochemical performance with a rapid I–V response. For different scan rates, all the curves observed almost in a triangular shape in the potential window between −0.9 V and 0 V.

This involves the current that flows through the working electrode and recording its voltage when the electrode is charged and discharged in a cyclic manner. Fig. 10a shows that the inclined curve for all the applied current and it indicates purely capacitive behaviour of ZnO/CNT nanocomposites. The gradual decrease of the voltage curve with respect to time indicates dissipation of energy from ZnO/CNT nanomaterial. Fig. 10 (b) Galvanostatic charge-discharge curves of CNT, ZnO and ZnO/CNT. It displays excellent electrochemical behaviour for ZnO/CNT.

Fig. 11 shows the electrochemical impedance spectroscopy (EIS) curve of ZnO/CNT based supercapacitor electrode in 1 M Na_2SO_4 electrolyte. It explains the impedance characteristic behaviour of ZnO/CNT based supercapacitor electrode, the ions of electrolyte diffusing into the active materials at the low-frequency region. If the slope of the plot was almost perpendicular, which indicates that ideal capacitive behaviour and good ionic conductivity [53].

Electrochemical impedance spectroscopy (EIS) measurements of ZnO/CNT nanocomposite have been performed in the frequency range from 0.1 Hz to 1 MHz. It is the evident of ion transfer mechanism of ZnO/CNT composite material. Fig. 11(a) shows that, EIS plot of ZnO/CNT nanocomposite in Na_2SO_4 electrolyte. The Nyquist plots Fig. 11(a) and (b), has three regions and also it has semi-circle with spike. These plots are filled in Z-view software and its equivalent circuits also shown in Fig. 11(a). The ohmic resistance/solution resistance (Rs) is assigned from intercept of the semicircle at high-frequency region and the x-axis value of semicircle indicates that, charge transfer resistance which are calculated using Z-view for ZnO, CNT and ZnO/CNT. In the low frequency region, a notable spike is observed due to the charge accumulation between interfaces of materials. Also, Nyquist plot gives ionic movement and ion diffusion in electrolyte (Z′) and charge accumulation behaviour with diffusion in the region of electrode and electrolyte interface (Z″) and it is given in Table 3. It is observed that, CNT and ZnO has high solution resistance and high charge transfer resistance, which indicates less ion diffusion and charge transfer. ZnO/CNT nanocomposite exhibits, lower value of ohmic resistance and charge transfer resistance. The specific lower charge transfer resistance results coincided with the observed rectangular redox peak CV curve. After 1000 cycles of charge and discharge of ZnO/CNT composite, the solution resistance and charge transfer resistance were increased; this declares that, reduction of charge diffusion in an electrolyte solution. In order to understand the life of the synthesised ZnO/CNT by chemical reflux method, it was examined in the plot between specific capacitance and retention of charge storage up to thousand cycles as shown in Fig. 12. Specific capacitance increases between the first 200 cycles for charge-discharge. But, around the 400thcycle, it decreases deeply and a similar observation was found in retention of charge. It is found that, after the 100th cycle, ZnO/CNT shows 96% of charge retention when the current density is increased from 1 to 5 mAg^{-1}, which is favourable for most applications.

Fig. 13 reveals that, the energy and power density of the ZnO/CNT electrode. It is important to note that, high power density 2250 W/Kg can be obtained at an energy density of 10.7 Wh/Kg. Also, an even higher energy density of 6.9 Wh/Kg, CNT exhibits about 450 W/Kg. Fig. 13 shows that the energy density is increased dramatically due to the formation of ZnO/CNT.

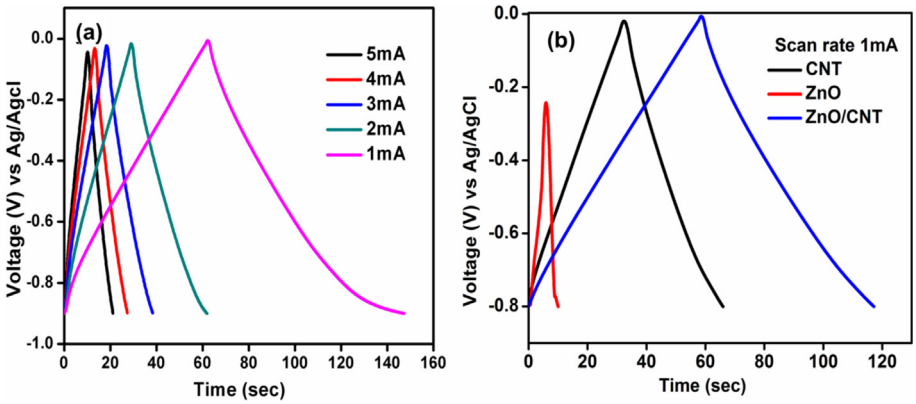

Fig. 10. (a). Galvanostatic charge-discharge curves of ZnO/CNT in different scan rates (b) Galvanostatic charge-discharge curves of CNT, ZnO and ZnO/CNT (scan rate in 1 mA).

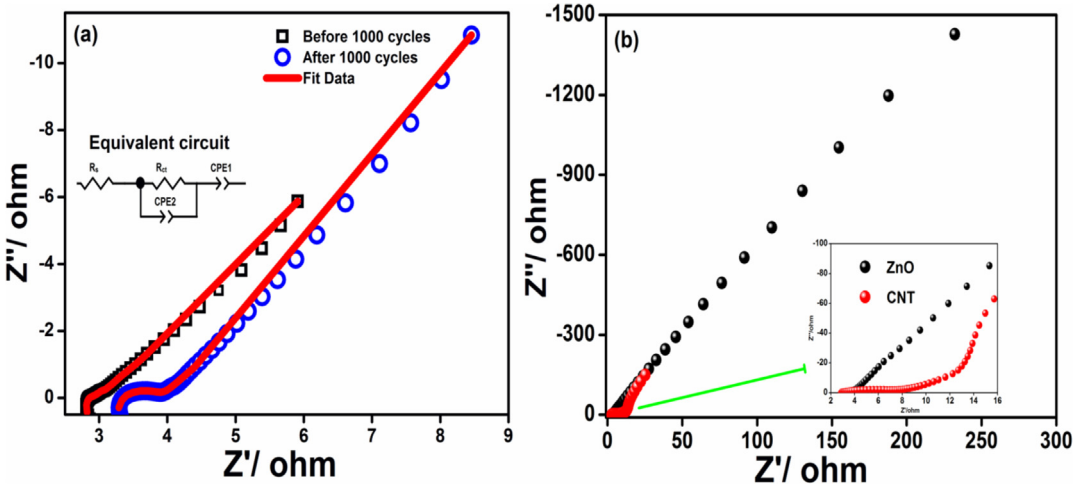

Fig. 11. (a) Impedance curves of ZnO/CNT composite (b) Impedance curves of ZnO and CNT.

Table 3
Ohmic resistance/solution resistance (R_s) and transfer resistances of the electrodes.

Materials	Ohmic resistance/solution resistance (R_s)	Transfer resistances
CNT	2.824	4.92
ZnO	3.511	200
ZnO@CNT Before 1000 cycles	2.76	0.17873
ZnO@CNT After 1000 cycles	3.214	0.6924

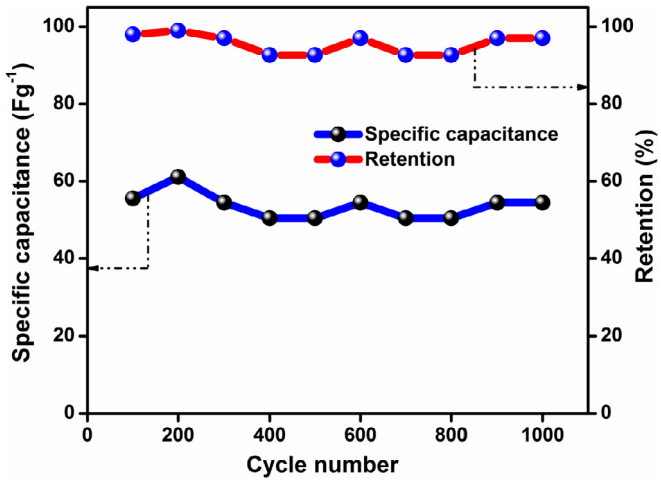

Fig. 12. Specific capacitance and retention life of ZnO/CNT for 1000 cycles.

Fig. 14, explains about the specific capacitance character of the electrode with respect to its current density. It shows that, when the current density increases, the specific capacitance decreases. Figs. 12 and 13 declare those ZnO/CNT electrodes are functioning with the higher power density and specific capacitance at lower current density, which is pre-requisite for supercapacitor applications.

4. Conclusions

ZnO nanorods have been grafted on the functionalized CNT surface successfully by the chemical refluxing method. The combination of ZnO nanorods and CNT in the synthesised ZnO/CNT nanocomposites has resulted in effective electrochemical performance. The FT-IR and

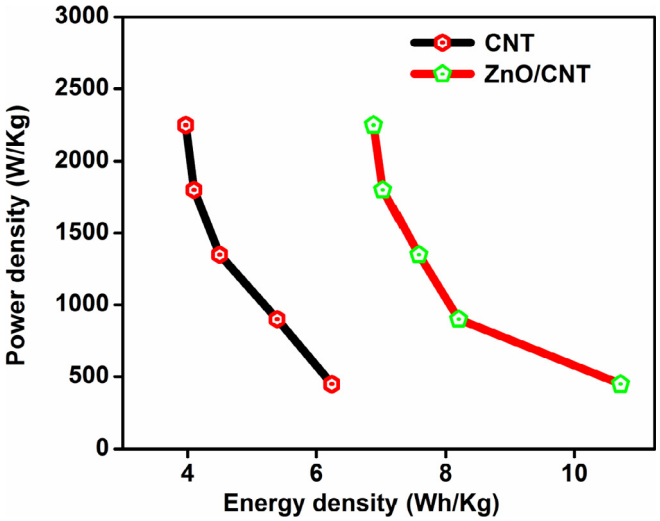

Fig. 13. Ragone plot of energy density Vs. power density of ZnO/CNT composite.

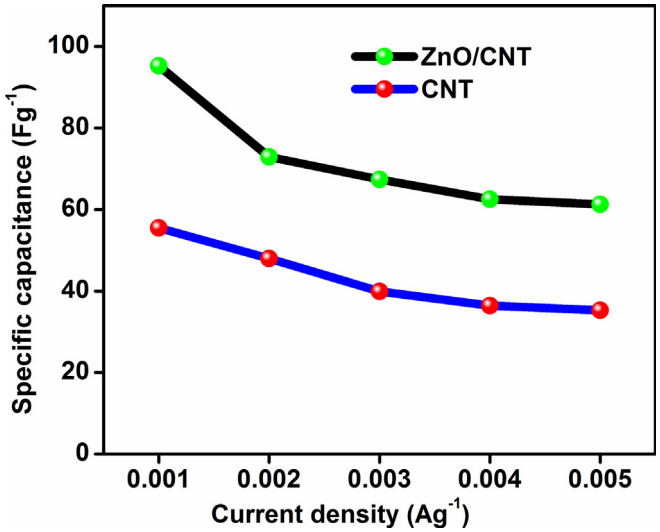

Fig. 14. Plot between Current density vs. specific capacitance of ZnO/CNT electrode.

Raman results confirmed the several stages of the synthesis of ZnO/CNT nanocomposites. The XRD study revealed that there exists a long-range order in CNT while ascertaining the crystallinity of ZnO nanorods. SEM image clearly shows the formation of ZnO nanorods embedded on the CNT surface in a uniform manner. The ZnO/CNT based supercapacitor has been investigated by three electrodes electrochemical workstation with 1 M Na_2SO_4 electrolyte. The specific capacitance of ZnO/CNT was calculated about 189 F/g at 1 mV s^{-1} scan rate. The shape of the CV curve confirms that, electric double layer capacitance (EDLC) behaviour of ZnO/CNT. The cyclic life for 1000 cycles declared that 96% retention of capacitance is achieved. Also, it exhibits higher power density about 2250 W/Kg for the energy density of 10.7 Wh/Kg. The results of CV, specific capacitance, charge-discharge curves and retention studies corroborate very well to assure the versatile applicability of ZnO/CNT nano-composite materials towards supercapacitors.

Acknowledgements

Author R.R has gratefully thanked Kalasalingam Academy of Research and Education (KARE) for given University Research Fellowship (URF) and also authors are grateful to IRC, KARE for providing research facilities. Also, financial assistance from DST-SERB (TARE), India through the Research Project (TAR/2018/001323) is gratefully acknowledged by N. Nallamuthu.

References

[1] B.K. Kim, Sy Serubbable, Aiping Yu, J. Zhang, Handbook of Clean Energy Systems, John Wiley & Sons, Ltd, 2015, pp. 1–25.
[2] M. Yassine, D. Fabris, Performance of commercially available supercapacitors, Energies 10 (2017) 1340 https://doi.org/10.3390/en10091340.
[3] L. Kouchachvili, W. Yaici, E. Entchev, Hybrid battery/supercapacitor energy storage system for the electric vehicles, J. Power Sources 374 (2018) 237–248 https://doi.org/10.1016/j.jpowsour.2017.11.040.
[4] F. Un-Noor, S. Padmanaban, L.M. Popa, M.N. Mollah, E. Hossain, A comprehensive study of key electric vehicle (EV) components, technologies, challenges, Impacts, and future direction of development, Energies 10 (2017) 1217 https://doi.org/10.3390/en10081217.
[5] B.G. Polleta, I. Staffell, Jin Lei Shang, Construction of one-dimensional nanostructures on graphene for efficient energy conversion and storage, Electrochim. Acta 84 (2012) 235 https://doi.org/10.1039/C4EE00531G.
[6] S. Faraji, F.N. Ani, The development supercapacitor from activated carbon by the electroless plating-A review, Renew. Sustain. Energy Rev. 42 (2015) 823–834 https://doi.org/10.1016/j.rser.2014.10.068.
[7] S.H. Kazemi, B. Hosseinzadeh, H. Kazemi, M.A. Kiani, S.H. Will, Facile synthesis of mixed metal-organic frameworks: electrode materials for supercapacitors with excellent areal capacitance and operational stability, ACS Appl. Mater. Interfaces 10 (27) (2018) 23063–23073 https://doi.org/10.1021/acsami.8b04502.
[8] M.F. El-Kady, M. Ihns, M. Li, J.Y. Hwang, M.F. Mousavi, L. Chaney, A.T. Lech, R.B. Kaner, Engineering three-dimensional hybrid supercapacitors and micro supercapacitors for high-performance integrated energy storage, Proc. Natl. Acad. Sci. Unit. States Am. 112 (14) (2015) 4233–4238. April 7 https://doi.org/10.1073/pnas.1420398112.
[9] Z.A. Rahim, N.A. Yusof, M.A.S.M. Haniff, F. Mohammad, M.I. Syono, N. Daud, Electrochemical measurements of multiwalled carbon nanotubes under different plasma treatments, Materials 1902 (1–11) (2018) 11 https://doi.org/10.3390/ma11101902.
[10] Q. Ke, J. Wang, Graphene-based materials for supercapacitor electrodes – a review, Journal of Materiomics 2 (1) (2016) 37–54 https://doi.org/10.1016/j.jmat.2016.01.001.
[11] N. Elgrishi, K.J. Rountree, B.D.M. Carthy, E.S. Rountree, T.T. Eisenhart, J.L. Dempsey, A practical beginner's guide to cyclic voltammetry, J. Chem. Educ. 95 (2018) 197–206 https://doi.org/10.1021/acs.jchemed.7b00361.
[12] X. Luo, J. Wang, M. Dooner, J. Clarke, Overview of current development in electrical energy storage technologies and the application potential in power system operation, Appl. Energy 137 (1) (2015) 511–536 https://doi.org/10.1016/j.apenergy.2014.09.081.
[13] C. Li, X. Zhang, K. Wang, X. Sun, G. Liu, J. Li, H. Tian, J. Li, Y. Ma, Scalable self-propagating high-temperature synthesis of graphene for supercapacitors with superior power density and cyclic stability, Adv. Mater. 29 (2017) 1604690 https://doi.org/10.1002/adma.201604690.
[14] S. Faraji, F.N. Ani, Microwave-assisted synthesis of metal oxide/hydroxide composite electrodes for high power supercapacitors – a review, J. Power Sources 263 (2014) 338–360 https://doi.org/10.1016/j.jpowsour.2014.03.144.
[15] A. Burke, Ultracapacitors: why, how, and where is the technology, J. Power Sources 91 (2000) 37–50 https://doi.org/10.1016/S0378-7753(00)00485-7.
[16] M. Selvakumar D.K. Bhat, A. Manish Aggarwal, S. Prahladh Iyer, G. Sravani, Nano ZnO-activated carbon composite electrodes for supercapacitors, Physica B 405 (2010) 2286–2289 https://doi.org/10.1016/j.physb.2010.02.028.
[17] S. Chen, W. Xing, J. Duan, X. Hu, S.Z. Qiao, Nanostructured morphology control for efficient supercapacitor electrodes, J. Mater. Chem. A 1 (2013) 2941–2954 https://doi.org/10.1039/C2TA00627H.
[18] H. Quan, B. Cheng, Y. Xiao, S. Lei, One-pot synthesis of α-Fe2O3 nanoplates-reduced graphene oxide composites for supercapacitor application, Chem. Eng. J. 286 (2016) 165–173 https://doi.org/10.1016/j.cej.2015.10.068.
[19] K. Balasubramanian, Chemically functionalized carbon nanotubes, Marko Burghard 1 (2005) 180–192 https://doi.org/10.1002/smll.200400118.
[20] G.Y. Li, P.M. Wang, X. Zhao, Mechanical behavior and microstructure of cement composites incorporating surface-treated multi-walled carbon nanotubes, Carbon 43 (2005) 1239–1245 https://doi.org/10.1016/j.carbon.2004.12.017.
[21] D. Tasis, N. Tagmatarchis, A. Bianco, M. Prato, Chemistry of carbon nanotubes, Chem. Rev. 106 (2006) 1105–1136 https://doi.org/10.1021/cr050569o.
[22] N. Karousis, N. Tagmatarchis, Current progress on the chemical modification of carbon nanotubes, Chem. Rev. 110 (2010) 5366–5397 https://doi.org/10.1021/cr100018g.
[23] T.M. Higgins, D. McAteer, J.C.M. Coelho, B.M. Sanchez, Z. Gholamvand, G. Moriarty, N. McEvoy, N.C. Berner, G.S. Duesberg, V. Nicolosi, J.N. Coleman, Effect of percolation on the capacitance of supercapacitor electrodes prepared from composites of manganese dioxide nanoplatelets and carbon nanotubes, ACS Nano 8 (2014) 9567–9579 https://doi.org/10.1021/nn5038543.
[24] Li Li, Zhong A. Hu, An Ning, Yu Y. Yang, Zhi M. Li, Hong Y. Wu, Facile synthesis of MnO_2/CNTs composite for supercapacitor electrodes with long cycle stability, J. Phys. Chem. C 118 (2014) 22865–22872 https://doi.org/10.1021/jp505744p.
[25] Y. Yang, Y. Liang, Z. Zhang, Y. Zhang, H. Wu, Z. Hu, Morphology well-controlled synthesis of NiO by solvothermal reaction time and their morphology-dependent pseudocapacitive performances, J. Alloy. Comp. 658 (2016) 621–628 https://doi.org/10.1016/j.jallcom.2015.10.253.
[26] K. Wang, X. Yi, X. Luo, Y. Shi, J. Xu, Fabrication of Co_3O_4 pseudocapacitor electrodes from nanoscale cobalt–organic frameworks, Polyhedron 109 (2016) 26–32 https://doi.org/10.1016/j.poly.2016.01.046.
[27] J. Choi, M. Kim, J. Kim, Synergistic interaction between embedded Co_3O_4 nanowires and graphene papers for high performance capacitor electrodes, RSC Adv. 7 (2017) 23793 https://doi.org/10.1039/C7RA02867A.
[28] N.S. Arul, J. In Han, Enhanced pseudocapacitance of $NiSe_2$/$Ni(OH)_2$ nanocomposites for supercapacitor electrode, Mater. Lett. 234 (2019) 87–91 https://doi.org/10.1016/j.matlet.2018.09.064.
[29] H. Wang, H.S. Casalongue, Y. Liang, H. Dai, $Ni(OH)_2$ nanoplates grown on graphene as advanced electrochemical pseudocapacitor materials, J. Am. Chem. Soc. 132 (2010) 7472–7477 https://doi.org/10.1021/ja102267j.
[30] T. Deng, W. Zhang, O. Arcelus, J.G. Kim, J. Carrasco, S.J. Yoo, W. Zheng, J. Wang, H. Tian, H. Zhang, X. Cui, T. Rojo, Atomic-level energy storage mechanism of cobalt hydroxide electrode for pseudocapacitors, Nat. Commun. 8 (2017) 15194 https://doi.org/10.1038/ncomms15194.
[31] C. Zhan, D. Jiang, Understanding the pseudocapacitance of RuO_2 from joint density functional theory, J. Phys. Condens. Matter 28 (2016) 464004 https://doi.org/10.1088/0953-8984/28/46/464004/meta.
[32] J. Hu, L. An, Q. Ren, W. Li, K. Xu, Y. Cao, T. Ji, R. Zou, Z. Chen, Highly ordered mesoporous $NiCo_2O_4$ with superior pseudocapacitance performance for supercapacitors, J. Mater. Chem. A (2015), https://doi.org/10.1039/C5TA01746G.
[33] L.S. Aravinda, K.K. Nagaraja, H.S. Nagaraja, K. Udaya Bhat, B. Ramachandra Bhat, ZnO/carbon nanotube nanocomposite for high energy density supercapacitors Electrochim, Acta 95 (2013) 119 https://doi.org/10.1016/j.electacta.2013.02.027.
[34] N.I.T. Ramli, S.A. Rashid, M.S. Mamat, Y. Sulaiman, S.A. Zobir, S. Krishnan, Incorporation of Zinc Oxide into Carbon nanotube/Graphite nanofiber as high performance supercapacitor electrode, Electrochim. Acta 228 (2017) 259 https://doi.org/10.1016/j.electacta.2017.01.068.
[35] Y. Zhang, X. Sun, L. Pan, H. Li, Z. Sun, C. Sun, B.K. Tay, et al., Carbon nanotube-zinc oxide electrode and gel polymer electrolyte for electrochemical supercapacitors, J. Alloy. Comp. 480 (2009) L17–L19 https://doi.org/10.1016/j.jallcom.2009.01.114.
[36] N. Venugopal, Yang, T. Ko, ZnO/CNT nanocomposite electrode for aqueous electrochemical supercapacitor, Mater. Res. Innov. 16 (2) (2013) 96–100 https://doi.org/10.1179/1433075x11y.0000000036.
[37] K.S. Lee, M.J. Shinb, C.W. Parka, J.D. Kim, Simple and direct synthesis of ZnO decorated multi-walled carbon nanotube for supercapacitor electrodes, Colloid. Surf. Physicochem. Eng. Asp. 538 (2018) 23–27 https://doi.org/10.1016/j.colsurfa.2017.10.075.
[38] A. Subagio, A. Darari, I.S. Hakim, Pardoyo Priyono, A. Subhan, Preparation and characterization of carbon nanotube/graphite/zinc oxide composite as supercapacitor electrode material, Mater. Sci. Forum 929 (2018) 121–127 https://doi.org/10.4028/www.scientific.net/msf.929.121.
[39] H. Sadegh, R.S. Ghoshekandi, Functionalization of carbon nanotubes and its application in nanomedicine: a review, Nanomed. J. 2 (4) (2015) 231–248 https://doi.org/10.7508/nmj.2015.04.001.
[40] Y. Zhou, P. Jin, Y. Zhou, Y. Zhu, High-performance symmetric supercapacitors based on carbon nanotube/graphite nanofiber nanocomposites, Sci. Rep. 8 (2018) 9005 https://doi.org/10.1038/s41598-018-27460-8.
[41] C. Lu, F. Su, S. Hu, Surface modification of carbon nanotubes for enhancing BTEX adsorption from aqueous solutions, Appl. Surf. Sci. 254 (2008) 7035–7041 https://doi.org/10.1016/j.apsusc.2008.05.282.
[42] B. Liu, H.C. Zeng, Hydrothermal synthesis of ZnO nanorods in the diameter regime of 50 nm, J. Am. Chem. Soc. 125 (2003) 4430–4431 https://doi.org/10.1021/ja0299452.
[43] K. Nakamoto, Infrared and Raman Spectra of Inorganic and Coordination

Compounds, Part B, Wiley, New York, 1997.
[44] S. Costa, E.B. Palen, Raman study on doped multiwalled carbon nanotubes, Acta Physics Polonica A 116 (2009) 32–35 https://doi.org/10.12693/APhysPolA.116.32.
[45] L. An, Q. Ren, W. Li, K. Xu, Y. Cao, T. Ji, R. Zou, Z. Chen, Highly ordered mesoporous NiCo 2 O 4 with superior pseudocapacitance performance for supercapacitors, J. Hu, J. Mater. Chem. A 3 (2015) 11503–11510 https://doi.org/10.1039/C5TA01746G.
[46] T. Palaniselvam, H.B. Aiyappa, S. Kurungot, An efficient oxygen reduction electrocatalyst from graphene by simultaneously generating pores and nitrogen doped active sites, J. Mater. Chem. 22 (2012) 23799–23805, https://doi.org/10.1039/C2JM35128E.
[47] N. Soin, S.S. Roy, S.C. Ray, J.A. McLaughlin, Excitation energy dependence of Raman bands in multiwalled carbon nanotubes, J. Raman Spectrosc. 41 (2010) 1227–1233 https://doi.org/10.1002/jrs.2594.
[48] J. Khan, S. Ilyas, B. Akram, K. Ahmad, M. Hafiz, M. Siddiq, M.A. Ashraf, Arabian ZnO/NiO coated multi-walled carbon nanotubes for textile dyes degradation, J. Chem. 11 (2018) 880–896 https://doi.org/10.1016/j.arabjc.2017.12.020.
[49] T.A. Saleh, S. Agarwal, V.K. Gupta, Synthesis of MWCNT/MnO2 and their application for simultaneous oxidation of arsenite and sorption of arsenate, Appl. Catal. B Environ. 106 (2011) 46–53 https://doi.org/10.1016/j.apcatb.2011.05.003.
[50] Z.A. Rahim, N.A. Yusof, M.A.S.M. Haniff, F. Mohammad, M. Syono, N. Daud, Electrochemical measurements of multiwalled carbon nanotubes under different plasma treatments, Materials 11 (2018) 1902 https://doi.org/10.3390/ma11101902.
[51] C.H. Kim, B.H. Kim, Zinc oxide/activated carbon nanofiber composites for high-performance supercapacitor electrodes, J. Power Sources 274 (2015) 512–520 https://doi.org/10.1016/j.jpowsour.2014.10.126.
[52] X. Lang, A. Hirata, T. Fujita, M. Chen, Nanoporous metal/oxide hybrid electrodes for electrochemical supercapacitors, Nat. Nanotechnol. 6 (2011) 232–236 https://doi.org/10.1038/NNANO.2011.13.
[53] S.H. Aboutalebi, A.T. Chidembo, M. Salari, K. Konstantinov, D. Wexler, H.K. Liu, S.X. Dou, Comparison of GO, GO/MWCNTs composite and MWCNTs as potential electrode materials for supercapacitors, Energy Environ. Sci. 4 (2011) 1855 https://doi.org/1865.10.1039/C1EE01039E.